

The 2019 Marine Heatwave at Ocean Station Papa: A multi-disciplinary assessment of ocean conditions and impacts on marine ecosystems

Catherine Kohlman¹, Meghan F. Cronin², Robert P. Dziak³, David K. Mellinger⁴, Adrienne J. Sutton⁵, Moira Galbraith⁶, Marie Robert⁷, Jim Thomson¹, Zhang Dongxiao⁸, and LuAnne Thompson¹

¹University of Washington

²NOAA PMEL

³NOAA/PMEL

⁴Oregon State University

⁵NOAA Pacific Marine Environmental Laboratory

⁶Institute of Ocean Science

⁷Fish and Oceans CA

⁸NOAA/PMEL and JISAO/UW, Seattle, USA,

July 8, 2023

Abstract

In the past decade, two large marine heatwaves (MHWs) formed in the northeast Pacific near Ocean Station Papa (OSP), one of the oldest oceanic time series stations. Physical, biogeochemical and biological parameters observed at OSP from 2013 to 2020 are used to assess ocean response and potential impacts on marine life from the 2019 northeast Pacific MHW. The 2019 MHW was preceded by calm and stratified surface conditions, lower dissolved inorganic carbon, and higher pH of surface waters relative to the 2013-2020 period. A spike in the summertime chlorophyll followed by a decrease in surface macronutrients suggests increased productivity in the well-lit stratified upper ocean during summer 2019. More blue whale calls were recorded at OSP in 2019 compared to the prior year. Large subsurface temperature anomalies were also found, suggesting that the earlier northeast Pacific MHW (2013-2015, previously referred to as “Blob”) as well as the long-term increase in sea surface temperatures in the region contributed to the intensity of the 2019 MHW. This study shows how the utility of long-term, continuous oceanographic datasets and analysis with an interdisciplinary lens is necessary to understand the potential impact of MHWs on marine ecosystems.

Hosted file

966833_0_art_file_11117468_rw6l8c.docx available at <https://authorea.com/users/633226/articles/651717-the-2019-marine-heatwave-at-ocean-station-papa-a-multi-disciplinary-assessment-of-ocean-conditions-and-impacts-on-marine-ecosystems>

Hosted file

966833_0_supp_11117438_rwcjd4.docx available at <https://authorea.com/users/633226/articles/651717-the-2019-marine-heatwave-at-ocean-station-papa-a-multi-disciplinary-assessment-of-ocean-conditions-and-impacts-on-marine-ecosystems>

1
2 **The 2019 Marine Heatwave at Ocean Station Papa: A multi-disciplinary assessment**
3 **of ocean conditions and impacts on marine ecosystems**
4

5 **Catherine Kohlman^{1*}, Meghan F. Cronin², Robert Dziak³, David Mellinger³, Adrienne**
6 **Sutton², Moira Galbraith⁴, Marie Robert⁴, Jim Thomson⁵, Dongxiao Zhang^{2,6}, and LuAnne**
7 **Thompson¹**

8
9 ¹University of Washington, School of Oceanography, Seattle, WA, USA

10 ²National Oceanic and Atmospheric Administration, Pacific Marine Environmental Laboratory,
11 Seattle, WA, USA

12 ³National Oceanic and Atmospheric Administration, Pacific Marine Environmental Laboratory,
13 Newport, OR, USA

14 ⁴Fisheries and Oceans Canada, Institute of Ocean Sciences, BC, Canada

15 ⁵University of Washington, Applied Physics Laboratory, Seattle, WA, USA

16 ⁶University of Washington, Cooperative Institute for Climate, Ocean, and Ecosystem Studies,
17 Seattle, WA, USA

18
19 * **Correspondence:** Catherine Kohlman (kohlman@uw.edu)

20 **Key Points:**

- 21 • The 2019 northeastern Pacific marine heatwave had various offshore physical,
22 biogeochemical, and biological impacts.
23 • Warm subsurface temperature anomalies suggest a connection between the 2013-2015
24 “Blob” and the 2019 “Blob2.0” marine heatwaves.
25 • Long-term multidisciplinary observing systems are necessary to provide a holistic view
26 of extreme events.
27

28 **Abstract**

29 In the past decade, two large marine heatwaves (MHWs) formed in the northeast Pacific near
30 Ocean Station Papa (OSP), one of the oldest oceanic time series stations. Physical,
31 biogeochemical and biological parameters observed at OSP from 2013 to 2020 are used to assess
32 ocean response and potential impacts on marine life from the 2019 northeast Pacific MHW. The
33 2019 MHW was preceded by calm and stratified surface conditions, lower dissolved inorganic
34 carbon, and higher pH of surface waters relative to the 2013-2020 period. A spike in the
35 summertime chlorophyll followed by a decrease in surface macronutrients suggests increased
36 productivity in the well-lit stratified upper ocean during summer 2019. More blue whale calls
37 were recorded at OSP in 2019 compared to the prior year. Large subsurface temperature
38 anomalies were also found, suggesting that the earlier northeast Pacific MHW (2013-2015,
39 previously referred to as “Blob”) as well as the long-term increase in sea surface temperatures in
40 the region contributed to the intensity of the 2019 MHW. This study shows how the utility of
41 long-term, continuous oceanographic datasets and analysis with an interdisciplinary lens is
42 necessary to understand the potential impact of MHWs on marine ecosystems.

43 **Plain Language Summary**

44 Marine heatwaves (MHWs) are extremely warm temperature events in the ocean. In 2019, a
45 MHW occurred in the northeastern Pacific, and we utilized Ocean Station Papa (OSP), a
46 multidisciplinary observing system in the Gulf of Alaska, to present the physical,
47 biogeochemical, and biological impacts. Prior to reaching the MHW’s peak surface
48 temperatures, the upper ocean exhibited a calm and stratified state, which facilitated the
49 occurrence of exceptionally high sea surface temperatures. During and after the extreme surface
50 temperatures were observed at OSP, warm water was present well below the surface, extending
51 throughout the water column. Prior to the MHW’s peak surface temperatures, we also observed
52 indications of increased primary productivity through observed spikes in chlorophyll levels and
53 reductions in nutrient concentrations. Due to data limitations, the connection between this
54 heightened primary productivity and higher trophic levels remains unclear. Our study
55 demonstrates the necessity of adopting holistic perspectives when seeking to understand the
56 complexities of MHWs.

57 **1 Introduction**

58 Prolonged extreme sea surface temperature (SST) anomalies, or marine heatwaves
59 (MHWs) (Hobday et al., 2016), are known to have a cascade of impacts on the ocean’s physics,
60 biogeochemistry, ecosystem and marine life. MHWs are often examined using either models or
61 satellite SST (Amaya et al., 2020; Bond et al., 2015; Capotondi et al., 2022; Holbrook et al.,
62 2019), ocean color (Hayashida et al., 2020; Noh et al., 2022), gridded subsurface data (Scannell
63 et al., 2020) or disparate observations (Bond et al., 2015). Here, we examine the 2019 MHW in
64 the northeast (NE) Pacific using a long-term ocean time series from the Ocean Station Papa
65 (OSP) observing node located near the epicenter of the NE Pacific MHWs. The meteorological,
66 physical, biogeochemical, and lower and higher trophic biological data enable us to consider the
67 connections that can result in widespread biogeochemical and ecosystem impacts.

68

69 In the recent decade, two notable MHWs (Hobday et al., 2016) have been observed in the
70 NE Pacific surrounding OSP. In the winter of 2013/2014, a MHW named the “Blob” was
71 observed and persisted well into 2015 (Bond et al., 2015) with subsurface temperature and

72 salinity anomalies lingering until 2018 (Scannell et al., 2020). The main drivers of the 2013-2015
73 MHW were weaker surface winds that resulted in weaker than normal surface heat loss and
74 weaker cold advection (Bond et al., 2015). Teleconnections from the Tropical Pacific likely
75 forced these atmospheric anomalies (Bond et al., 2015; Capotondi et al., 2022; Di Lorenzo &
76 Mantua, 2016; Hartmann, 2015; Holbrook et al., 2019; Holbrook et al., 2020). Based upon OSP
77 biogeochemical observations from 2007 through 2018, Mogen et al. (2022) suggest that these
78 2013-2015 MHW drivers were also responsible for an observed decrease in surface oxygen (O₂)
79 and dissolved inorganic carbon (DIC). The upper ocean changes associated with the 2013-2015
80 MHW had pronounced coastal and offshore impacts on marine biodiversity, ecosystems, and
81 fishery economics (Bond et al., 2015; Cheung & Frölicher, 2020; Holbrook et al., 2019; Long et
82 al., 2021; Smale et al., 2019).

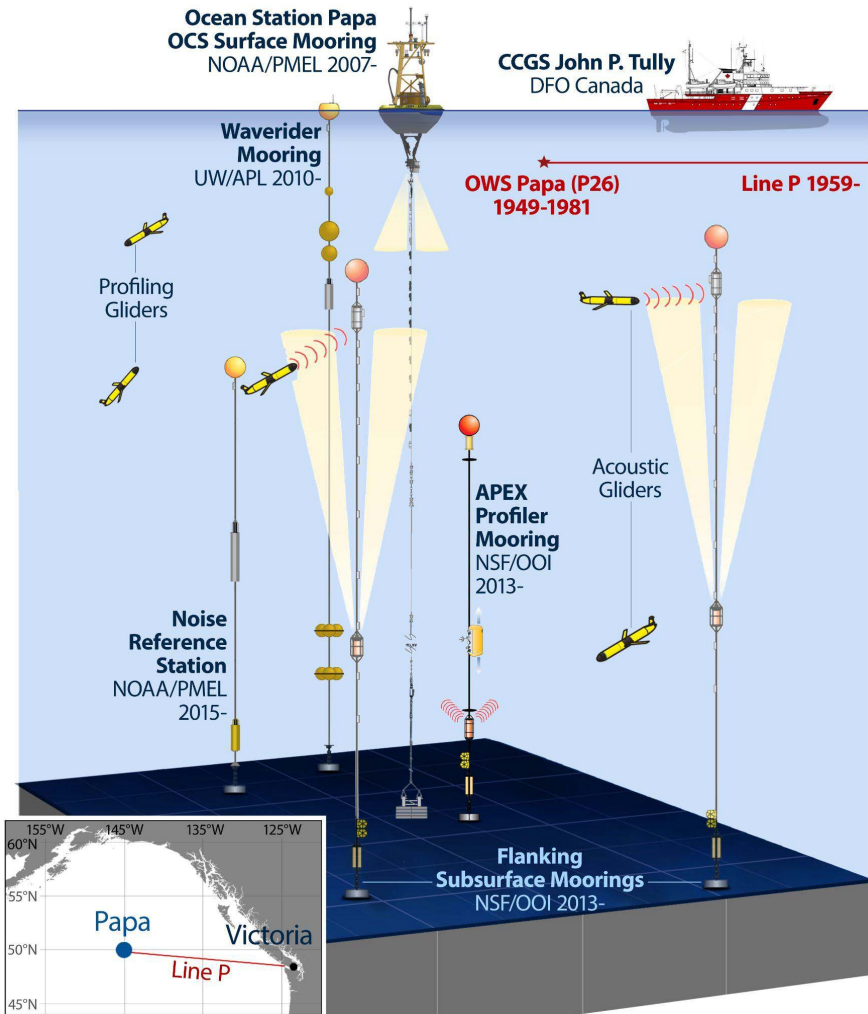
83

84 In 2019, after the SST anomalies of the 2013-2015 MHW dissipated, the NE Pacific
85 experienced another MHW, referred to as the “Blob2.0” (Amaya et al., 2020). Similar to the
86 2013-2015 MHW, the 2019 MHW appeared to be driven in part by reduced surface-level winds
87 resulting from large-scale atmospheric anomalies (Amaya et al., 2020). The 2019 MHW peaked
88 in the summer and had larger SST anomalies than the 2013-2015 MHW owing to positive net
89 surface heat fluxes and a record shallow mixed layer (Amaya et al., 2020). The entire water
90 column was fresher and more stratified than in the 2013-2015 MHW, and the 2019 MHW was
91 believed to be supercharged by reemerged subsurface temperature anomalies from the 2013-
92 2015 MHW (Scannell et al., 2020).

93

94 Located at 50°N, 145°W, 1200 km offshore of Vancouver Island, B.C. Canada, OSP
95 (Figure 1) is site of one of the oldest multi-disciplinary time series (Harrison, 2002; Whitney &
96 Freeland, 1999; Whitney et al., 1998) and is just north of the centers of the two aforementioned
97 MHWs (Figure 2ab). From 1949 through 1981 it was occupied by a weather ship and since 1956,
98 the Canadian Department of Fisheries and Oceans (DFO) Line P Program has made ship-based
99 oceanographic observations at OSP and along a transect from the coast to OSP. At present, Line
100 P ship-based observations are taken three times a year – typically in February, June and August
101 (Freeland, 2007). The NOAA Pacific Marine Environmental Laboratory (PMEL) Ocean Climate
102 Station (OCS) surface mooring time series began at OSP in June 2007. In 2010, a Waverider
103 surface mooring was deployed at OSP by the University of Washington (UW) Applied Physics
104 Laboratory (APL). In 2015, OSP was enhanced to become a global node of the National Science
105 Foundation (NSF) Ocean Observatory Initiative (OOI), with the deployment of two flanking
106 subsurface moorings and a subsurface profiling mooring. In 2015, NOAA deployed a Noise
107 Reference Station (NRS) that records passive acoustics for monitoring whales and other marine
108 mammals. Together, these time series allow for multi-disciplinary studies to understand the
109 evolution and impacts surrounding extreme events, such as MHWs.

110



111
 112 **Figure 1.** Illustration of the operational components of Ocean Station Papa and their respective
 113 names and locations. Credit: Sarah Battle, NOAA/PMEL graphic adapted from original by the
 114 Ocean Observatories Initiative.

115
 116 In this study, we use OSP as an open ocean natural laboratory to explore the ocean’s
 117 physical, chemical, and biological responses to the 2019 MHW forcing. We present a holistic
 118 study of the 2019 MHW that analyzes the surface and subsurface temperature and stratification
 119 anomalies, including the recovery from the 2013-2015 MHW. We examine the potential
 120 relationships between the increased surface temperature, increased stratification, reduced ocean
 121 acidification, increased productivity, and possible linkages to higher trophic levels at OSP in the
 122 summer of 2019. This case study provides insight into the complex interconnections and
 123 potential impacts of extreme ocean warming events.

124 **2 Materials and Methods**

125 **2.1. Identifying MHW periods at OSP**

126 We identified MHWs at OSP as events where the local 31-day boxcar filtered daily SST
 127 anomalies relative to the seasonal climatology exceed the 90th percentile, similar to the MHW

128 definition in Hobday et al. (2016). Gaps less than 5-days were linearly interpolated prior to
129 applying the 31-day filter. The climatology was calculated from the OSP NOAA surface
130 mooring 31-day filtered SST time series from 2007 to 2020.

131 The following list describes the suite of in-situ (moored and shipboard) and satellite data along
132 with methods for quantities that we used to assess the widespread multi-disciplinary effects of
133 the 2019 MHW. All climatologies are computed from a 31-day running average over the record
134 length ending on Dec 31, 2020. Climatologies for subsurface salinity and temperatures were
135 computed from nearby Argo floats profiles found within 49-51°N & 144-146°W between 1999
136 and 2022. All other climatologies are based upon the OSP time series. Anomalies on the 31-day
137 running average time series in moored and gridded quantities are computed relative to these
138 climatologies after filling gaps that are 5-days or less. Links to data sets used are found in the
139 Data Availability section.

140 **2.2 NOAA Surface Mooring**

141 **2.2.1. Surface Meteorological Variables, Temperature, Salinity, and Currents Data**

142 Air-sea flux state variables (downwelling solar and longwave radiation, winds, surface currents,
143 humidity, air and sea surface temperature, sea surface salinity, humidity, barometric pressure and
144 rain); upper ocean temperature (at 23 depths from 1 m to 300 m), salinity (at 21 depths from 1 m
145 to 300 m), computed potential density, and horizontal current time series at 35 m from the
146 NOAA surface mooring at OSP are provided by the Ocean Climate Stations (OCS) Group
147 (Cronin et al., 2015). Wind stress, evaporation, and latent and sensible heat fluxes are computed
148 hourly using the Fairall et al. (2003) COARE 3.0b algorithm, and net surface heat flux is
149 estimated as described in Cronin et al. (2015).

150 **2.2.2. Seawater $p\text{CO}_2$ and Surface pH**

151
152 Surface water $p\text{CO}_2$ (the partial pressure of CO_2 in air in equilibrium with the seawater at sea
153 surface temperature) and surface seawater pH time series are from the Pacific Marine
154 Environmental Lab (PMEL) Carbon Group (Sutton et al., 2016; Sutton et al., 2014; Sutton et al.,
155 2012). Both variables were collected autonomously every 3-hours.

156 **2.2.3. Bandpassing**

157 To obtain the near-inertial currents, we used a bandpass filter on 35 m hourly currents observed
158 at the OSP NOAA surface mooring by defining the high-pass of the triangular filter to be 7-hours
159 (~ 0.5 times the inertial period), and the low-pass of the filter was 1.5 times the inertial period (23
160 hours) at 50°N.

161 **2.2.4. Computing Dissolved Inorganic Carbon, Mixed Layer, and Saturation Equilibrium 162 Oxygen**

163 To analyze the carbon system during the study period, the surface dissolved inorganic carbon
164 (DIC) was computed from daily-averaged surface water $p\text{CO}_2$, surface pH, sea surface salinity,
165 and sea surface temperature from the NOAA surface mooring at OSP. The program used to
166 compute the surface DIC was the MATLAB-version (v1.1) of CO2SYS (Lewis & Wallace,

167 1998; van Heuven et al., 2011) with the borate-to-salinity ratio of Dickson (1990), sulfate
168 dissociation constants of Dickson (1990), and the carbonic acid dissociation constants of
169 Dickson and Millero (1987) - refit data of Mehrbach et al. (1973).

170 **2.2.5. Computing Mixed Layer**

171 The mixed layer depths at OSP were computed using methods described in Cronin et al. (2015)
172 using daily-averaged temperature and salinity profiles from the OSP surface mooring. Mixed
173 layer depth is defined as the depth where density is 0.03 kg m^{-3} denser than that found at 10 m
174 depth. An isothermal layer depth, defined as the depth where temperature is 0.2°C cooler than
175 found at 10 m depth, is also computed. A barrier layer exists when the mixed layer depth is
176 salinity stratified and shallower than the isothermal layer (Katsura et al., 2015; Lukas &
177 Lindstrom, 1991; de Boyer Montégut, 2004).

178 **2.2.6. Computing Saturation Equilibrium Oxygen**

179 The saturation equilibrium oxygen in seawater was computed using the Gibbs SeaWater (GSW)
180 Oceanographic MATLAB Toolbox (McDougall & Barker, 2011) with inputs of absolute salinity
181 (computed from density and in-situ temperature) and conservative temperature (computed from
182 absolute salinity and in-situ temperature). The GSW Toolbox uses solubility coefficients from
183 Benson and Krause Jr (1984) as fitted by Garcia and Gordon (1992, 1993).

184 **2.3. NSF OOI Subsurface Moorings**

185 Deep (300-1500 m) subsurface temperature and salinity observations were provided by the NSF
186 OOI Global Station Papa Array's Flanking Moorings A and B. These two flanking moorings are
187 located within 60 km of the NOAA surface mooring and contain CTDs collecting data every 15
188 minutes at discrete depths from 30 m below the surface to 1500 m. Deep (300-1500 m) profiles
189 (Figure 3a) were created by averaging the daily-averaged values between the Flanking
190 Subsurface Moorings A and B.

191 **2.4. APL-UW Waverider Mooring**

192 Daily significant wave height time series data from the Waverider mooring at OSP were
193 provided by the APL-UW Waverider Group. The Waverider collects pitch roll and heave
194 displacements at 1.28 Hz at 30-minute intervals (Thomson et al., 2013). Spectral moments are
195 computed onboard and then transmitted to the Coastal Data Information Program (CDIP) at the
196 Scripps Institution of Oceanography. These buoy data are publicly available as CDIP Station 166
197 and National Data Buoy Center (NDBC) Station 46246.

198 **2.5. Ship Data**

199 **2.5.1. DFO Line P shipboard data**

200 Station P26, at OSP, is the farthest offshore station of the "Line P" survey line. This study
201 includes *Euphausia pacifica* dry weight biomass (from *E. pacifica* abundance; Mackas, 1995),
202 chlorophyll concentrations, nitrate plus nitrite (nitrite measurements are so small, $<0.3 \mu\text{M}$, that
203 nitrate plus nitrite can be expressed as nitrate for simplicity; Whitney et al., 1998), sulfite, and

204 oxygen observations at Station P26 for insight into biological activity at OSP. Data displayed as
205 ‘surface’ refers to the depth integrated values from the air-sea interface to 5 m depth. There are
206 three Line P cruises per year generally in February, June, and August. The Line P data are
207 managed and coordinated by the Institute of Ocean Sciences from Fisheries and Oceans Canada
208 (DFO). Data submitted to PACIFICA from NCEI (Suzuki et al., 2013), within 49-51°N & 144-
209 146°W, are used as a 1985-2008 climatology for nitrate plus nitrite, sulfite, and oxygen.

210 **2.5.2. OOI Various Cruises**

211 Supplemental chlorophyll, oxygen, nitrate plus nitrite, and sulfite cruise ship samples at OSP are
212 included from OOI’s shipboard data log ranging from July 2013 to present with about one cruise
213 per year, generally in late summer.

214 **2.6. NOAA Noise Reference Station Mooring: Autonomous Hydrophone Data and Whale** 215 **Call Detection**

216 The hydrophone recording package used to collect ambient acoustic data at the OSP Noise
217 Reference Station (NRS) subsurface mooring consists of a single ceramic hydrophone with a
218 filter/amplifier, clock, and a low-power processor, all powered by an internal battery pack. The
219 hydrophone (model ITC-1032) is omnidirectional with a nominal sensitivity of -192 dB re 1 V
220 μPa^{-1} . The instrument records at a sampling rate of 5 kHz with 16-bit resolution, providing a
221 continuous record of ocean ambient sound levels from July 2018 to September 2020. The pre-
222 amplifier has an eight-pole anti-aliasing filter at 2.5 kHz with a filter curve to equalize the
223 spectrum against typical ocean noise over the passband (Dziak et al., 2019). A low power cesium
224 atomic clock with an average time drift of ~ 0.1 s year $^{-1}$ was used for internal timing. The NRS
225 sensor was located at 900 m within the ocean sound channel, with the goal of maximizing the
226 detection range of biological sound sources.

227 The seasonal, acoustic presence of blue whales in the northeastern Pacific has been established in
228 previous studies using hydrophone recordings of their vocalizations (Stafford et al., 2009). To
229 detect recent blue whale call presence using the moored hydrophone at OSP, we used
230 spectrogram correlation techniques (Mellinger & Clark, 2000) to target the tonal parts of the blue
231 whale B call at signal frequencies between 25 and 26.5 Hz and time durations between 2.5 and
232 15 seconds in duration. The B call is suggested to be a result of pneumatic air bursts from the
233 whales opening and closing respiratory air valves and can be used to identify the presence of
234 blue whales (Dziak et al., 2017). The whale detection analysis was run in Ishmael (V.2.3.1)
235 (Mellinger, 2001) over the two years of continuous hydrophone data at OSP (2018-2020). To
236 identify the B call, a two-dimensional synthetic kernel is constructed and cross-correlated with a
237 spectrogram of a recording, producing a recognition function—the likelihood at each point in
238 time that the sound type was present. A threshold is then applied to this function to obtain
239 discrete detection events, which are discrete points in time when the B call was likely present.
240 The same spectrogram correlation method was used to detect sperm whale clicks, with the kernel
241 adjusted in frequency and time to capture the short duration (< 0.5 sec) broadband (~ 100 -500 Hz)
242 signal character of the clicks (Mellinger, 2004).

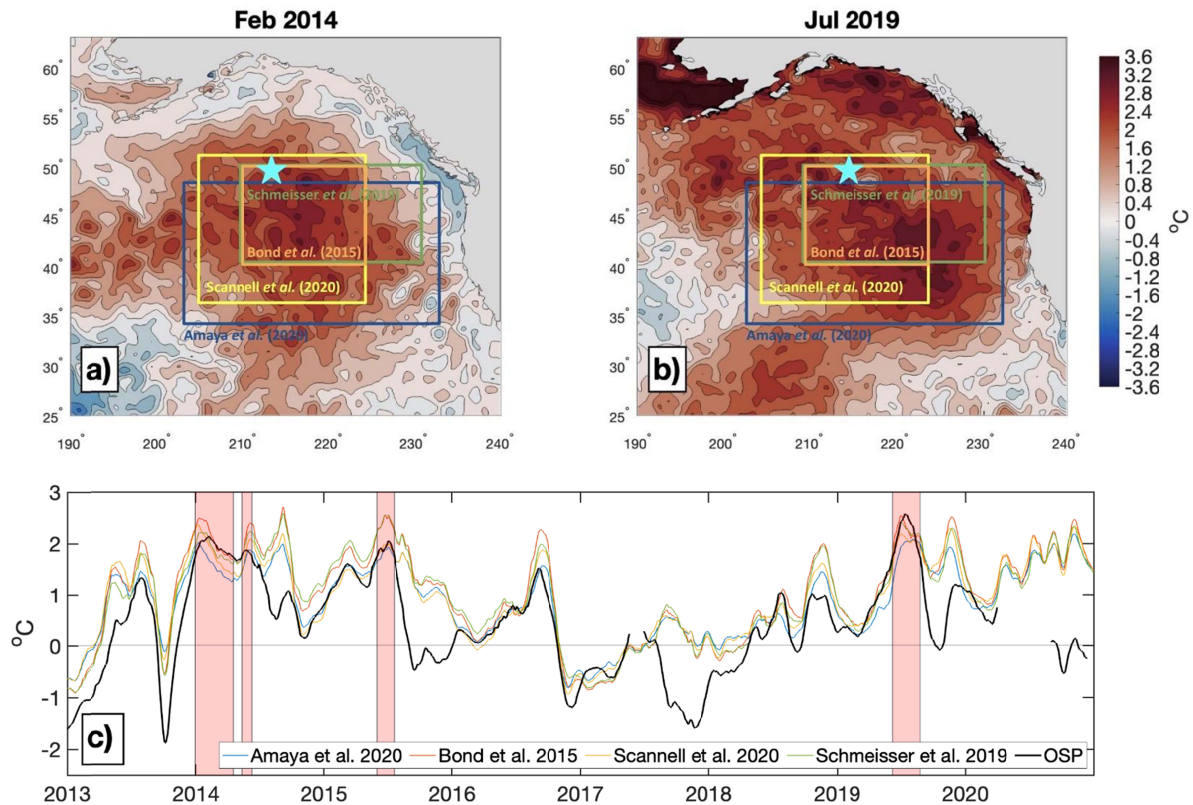
243 **2.7. Gridded SST Data**

244 The NOAA $\frac{1}{4}$ degree daily Optimum Interpolation Sea Surface Temperature (OISST) v2.1 data
245 (Huang et al., 2020) were used to display locations of SST anomalies associated with the 2013-
246 2015 and 2019 MHWs as well as a time series of SST anomalies associated with other studies,
247 computed from the 1982-2010 climatology. The OISSTv2.1 data available from September 1,
248 1981 until the present are a combination of observations from different satellites, ships, buoys,
249 and Argo floats interpolated to produce a spatially complete global SST map.

250 **3 Results**

251 **3.1. Surface and Subsurface Anomalies**

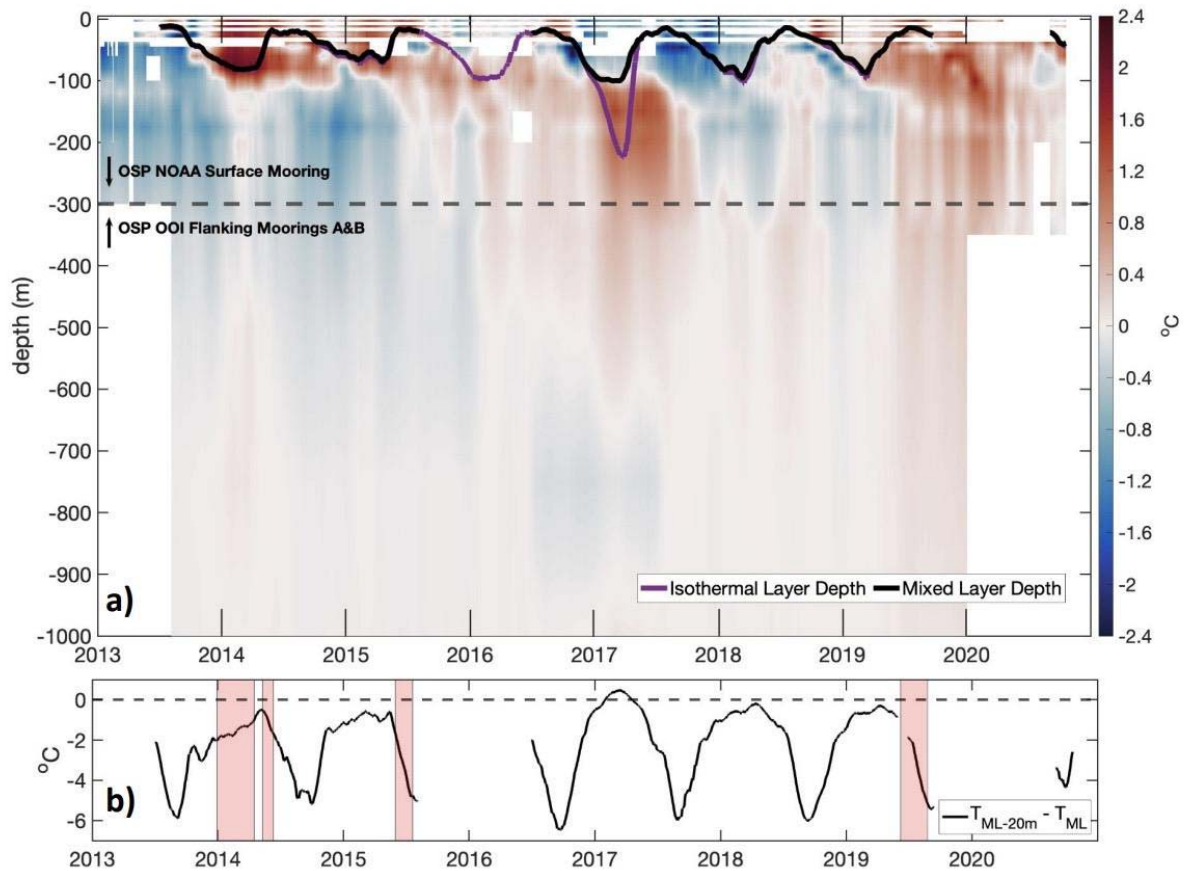
252
253 The general spatial pattern of SST anomalies for the 2013-2015 MHW (Figure 2a) and
254 the 2019 MHW (Figure 2b) are similar. The centers of each event are generally located south of
255 Anchorage, AK USA and west of Oregon USA. Centered in the Gulf of Alaska, OSP provides
256 in-situ observations that create a unique natural laboratory for understanding MHWs. Although
257 OSP is generally along the northernmost boundary for many area-averaged studies (Figure 2ab),
258 the observed SST anomalies at the NOAA surface mooring at OSP align well with area-averaged
259 studies using satellite data, identifying the periods of peak anomalies for each MHW (Figure 2c).
260 The red shading in the time series in Figure 2c represents MHW periods (see methods) that were
261 observed at the NOAA surface mooring (in black) and area averaged OISSTv2.1 SST anomalies
262 defined by various other studies (colored) from 2013 to 2020. During the 2013-2015 MHW
263 period, three MHW periods were observed at OSP, all part of the 2013-2015 MHW event. The
264 longest period of high SST anomalies at OSP occurred from Dec 30, 2013, to Apr 17, 2014, that
265 persisted for 109 days and reached a maximum SST anomaly of 2.1°C. The 2019 MHW was
266 observed at OSP from Jun 8, 2019, to Aug 25, 2019 (79 days) with a peak SST anomaly of
267 2.6°C.
268



269
 270 **Figure 2.** OISSTv2.1 daily sea surface temperature (SST) anomalies [$^{\circ}\text{C}$] during (a) Feb 2014
 271 and (b) Jul 2019. The blue star represents the location of OSP. (c) Observed SST anomalies from
 272 the NOAA surface mooring at OSP [$^{\circ}\text{C}$; black solid line] overlaid upon area-averaged SST
 273 anomalies [$^{\circ}\text{C}$] from OISSTv2.1 from areas defined in other studies (Amaya et al., 2020: 34–
 274 47 $^{\circ}\text{N}$ and 147–128 $^{\circ}\text{W}$; Bond et al., 2015: 40–50 $^{\circ}\text{N}$ and 150–130 $^{\circ}\text{W}$; Scannell et al., 2020: 35.5–
 275 51.5 $^{\circ}\text{N}$ and 154.5–135.5 $^{\circ}\text{W}$ and Schmeisser et al, 2019: 40–50 $^{\circ}\text{N}$ and 150–130 $^{\circ}\text{W}$) plotted in
 276 various colors (see legend). The red shading indicates ‘MHW periods’ (see methods). The tick
 277 marks on the horizontal axis are placed on Jan 1 of the year shown.

278
 279 Subsurface temperature anomalies recorded at the NOAA surface mooring and OOI
 280 subsurface moorings at OSP during the start of the first MHW in late 2013 and early 2014 were
 281 strongest above the mixed layer depth (MLD) (i.e., the black line in Figure 3a above ~100 m)
 282 and persisted until 2017. In the winter and spring of 2017, deeper waters (120–300 m) remained
 283 anomalously warm. Scannell et al. (2020) suggest that this deep warm temperature anomaly may
 284 be a signature of subducted warm surface anomalies from the 2013–2015 MHW. Further, this
 285 subsurface temperature anomaly persisted at least to 2018 and possibly regionally to 2019 as a
 286 result of being shielded from winter surface cooling by anomalously strong stratification and a
 287 fresher surface layer. As shown in Figure 3, during the winter of 2017 an extraordinarily thick
 288 “barrier layer”, approximately 140 m thick, is found at OSP along with a temperature inversion
 289 present from Feb 2017 to Apr 2017 (Figure 3b). Here we define a barrier layer when the MLD is
 290 salinity stratified and shallower than the isothermal layer (Katsura et al., 2015; Lukas &
 291 Lindstrom, 1991; de Boyer Montégut, 2004). Turbulent mixing and entrainment that eroded the
 292 MLD in this case caused the warm anomalies to re-emerge and “supercharge” the 2019 MHW.

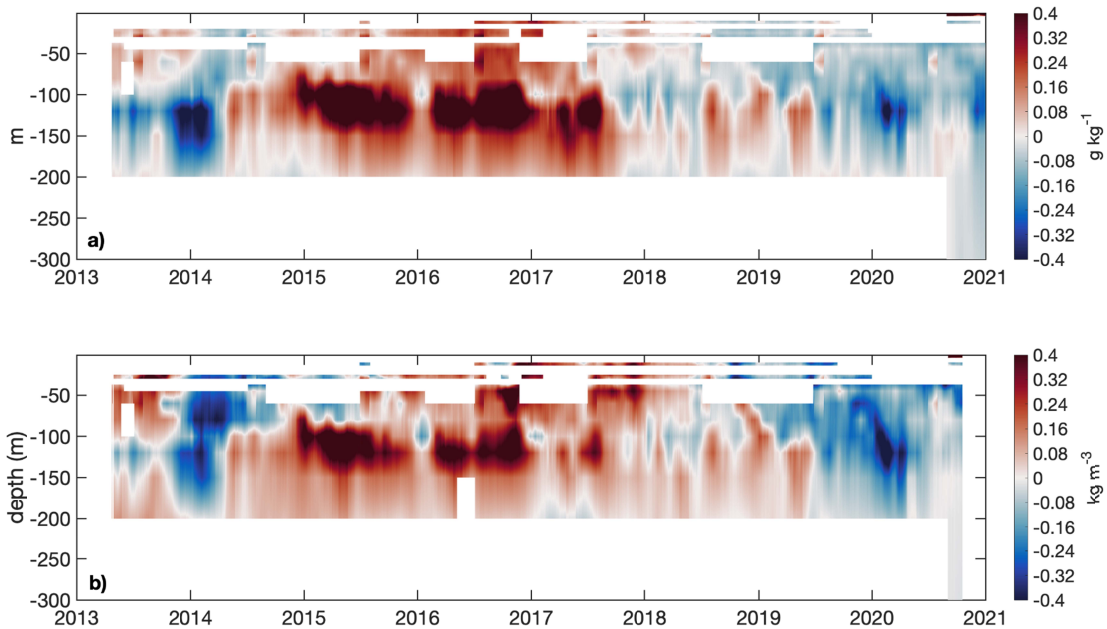
293 During the 2019 MHW, subsurface anomalously warm waters extended down to 1000 m, likely
 294 associated with a downward heaving of the thermocline associated with large-scale changes in
 295 the circulation.
 296



297 **Figure 3. (a)** Subsurface temperature anomalies [$^{\circ}\text{C}$] at OSP. Data from the surface to 300 m are
 298 from the OSP NOAA surface mooring, and data below 300 m are averaged from OSP OOI
 299 Flanking Moorings A and B. Subsurface anomalies computed from 1999-2020 Argo
 300 climatology. Base of deep isothermal layer [m; purple solid line] and base of shallow isopycnal
 301 mixed layer depth (MLD) [m; black solid line] are overlaid. **(b)** Temperature difference between
 302 the mixed layer and 20 m below the mixed layer [$^{\circ}\text{C}$]. Data are shown as a 31-day running
 303 average.
 304

305
 306 The upper ocean was anomalously stratified preceding the 2019 MHW (as early as mid-
 307 2018 to the summer of 2019), as seen by the anomalously less dense (blue) waters above the
 308 anomalously denser waters (red) in Figure 4b. Since mid-2017 onward, there were fresher than
 309 normal conditions in the upper 100 m of the ocean at OSP that overlie a warm subsurface
 310 temperature anomaly (Figure 4a). Scannell et al. (2020) suggest that these fresh anomalies were a
 311 result of increased freshwater input from precipitation in the Gulf of Alaska; however, there was
 312 not an increase in precipitation at OSP (Figure S1). Together, the surface ocean warm and fresh
 313 anomalies worked together to anomalously stratify the upper ocean in the winter of 2018/2019.
 314 The increase in stratification inhibited entrainment of deeper cooler waters, leading to favorable
 315 conditions for extreme SSTs.

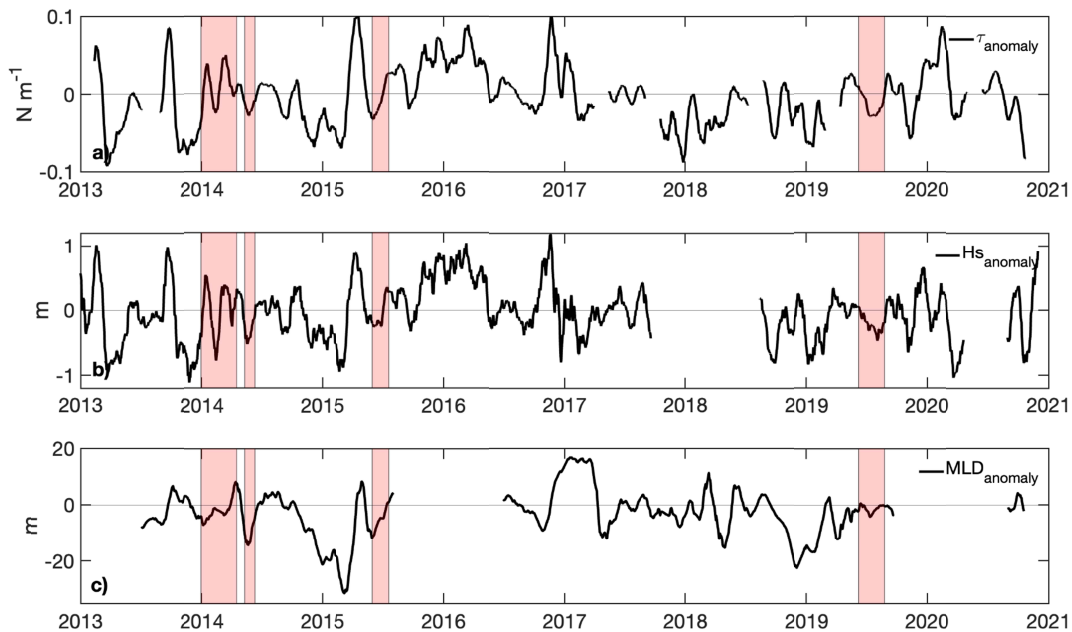
316



317
 318 **Figure 4. (a)** Subsurface salinity anomalies [g kg^{-1}] and **(b)** potential density anomalies [kg m^{-3}]
 319 computed from subsurface temperature and salinity profiles observed from the NOAA surface
 320 mooring at OSP. Subsurface anomalies computed from 1999-2020 ARGO climatology. Data are
 321 shown as a 31-day running average.

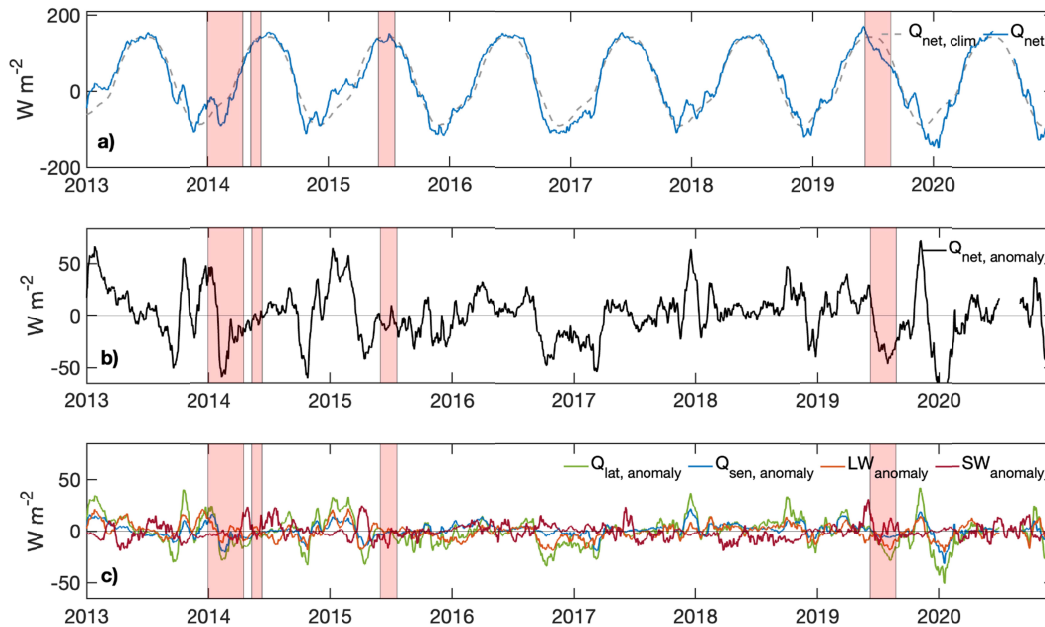
322
 323 Observed negative wind stress magnitude and significant wave height anomalies (Figure
 324 5ab) suggest calmer surface conditions that likely reduced wind-driven turbulence and mixing
 325 during the winter of 2018/2019 and summer of 2019. These significant wave height anomalies
 326 are also included here as an integral measure of the regional winds in that they include not only
 327 local wind generated waves, but also swell (Belka et al., 2014). The calmer conditions are also
 328 reflected by the anomalously shallower winter and summer MLD (Figure 5c). Although the OSP
 329 2019 summer MLD anomaly may appear small (5-6 m), the typical summer MLD (taken from
 330 the 2007-2020 climatology) at OSP reaches depths of about 10-13 m, suggesting roughly a 50%
 331 shoaling. The anomalously shallow winter mixed layer observed in 2018/2019 followed by
 332 reduction in wind-driven turbulence and shallow mixed layer in the summer of 2019 suggest a
 333 reduction of entrainment of cool, deeper waters into the upper ocean during the winter prior to
 334 the 2019 MHW, creating conditions favorable for warm upper ocean temperatures.

335



336
 337 **Figure 5.** (a) Wind stress [N m^{-2}] observed from the NOAA surface mooring, (b) significant
 338 wave height [m] observed from the APL-UW Waverider mooring, and (c) mixed layer depth [m]
 339 anomalies observed from the NOAA surface mooring at OSP. A negative mixed layer depth
 340 anomaly represents a shallower mixed layer. Data are shown as a 31-day running average. The
 341 red shading represents observed MHW periods.

342
 343 At OSP, the surface heat flux anomalies leading up to the 2019 MHW do not show as
 344 large a signal as anticipated (Figure 6) based on other air-sea flux analyses of the initiation of NE
 345 Pacific MHWs (Amaya et al., 2020; Schmeisser et al., 2019). These studies, which interpret the
 346 large anomalous net surface heat flux to be major drivers in the 2019 MHW were based on area-
 347 averaged studies with an emphasis on the region south of OSP (Figure 2ab). At OSP, the net heat
 348 fluxes were anomalously positive (into the ocean) in May and June of 2019 prior to the MHW
 349 (Figure 6ab), largely due to contributions from shortwave radiative fluxes (Figure 6c). During
 350 the 2019 MHW period, there was anomalous net heat flux out of the ocean, rather than into the
 351 ocean, as expected.

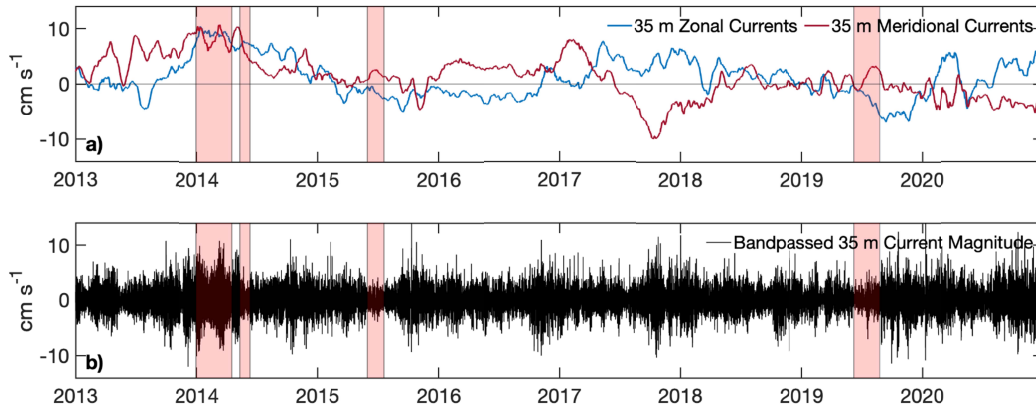


352
 353 **Figure 6.** (a) Net heat flux [$Q_{\text{net}} = SW_{\text{net}} - Q_{\text{lat}} - Q_{\text{sen}} - LW_{\text{net}}$], (b) net heat flux anomalies, and (c)
 354 latent heat flux anomalies (green), sensible heat flux anomalies (blue), longwave radiative
 355 anomalies (orange), and shortwave radiative anomalies (red) from the NOAA Surface Mooring
 356 at OSP. A positive flux anomaly warms the ocean. Data are shown as a 31-day running average.
 357 The red shading represents MHW periods.

358
 359 From early 2017 through winter 2019, the 35 m currents at OSP were generally eastward
 360 (positive zonal currents), in the direction of the North Pacific Current (Cummins & Freeland,
 361 2007). However, during the summer of 2019, there was a sudden weakening and shift from
 362 eastward to westward flow (Figure 7a). This shift from eastward to westward flow was not found
 363 during the 2013-2015 MHW. During the 2019 MHW, the changes in current direction may have
 364 reduced horizontal advection of cooler temperatures from west of OSP. Following this shift in
 365 zonal currents in mid-2019, the westward flow continued into the winter of 2019/2020. Although
 366 of lesser magnitude in summer 2019 compared to the 2013/2014 winter, there were also
 367 northward currents at OSP that might have advected warmer water into the region from the south
 368 (Figure 7a).

369
 370 Higher energy near-inertial waves are typically observed at OSP during the winter season
 371 owing to the increased frequency of storms in winter (Alford et al., 2012). At OSP, the 35 m
 372 near-inertial currents are largest from October to January (Figure 7b). However, during the
 373 winter 2018/2019, there were slightly smaller near-inertial currents (as seen by smaller high
 374 frequency currents in 2018/2019 winter compared to 2016/2017 and 2017/2018 winters). This
 375 suggests that the weaker winds and inertial currents resulted in a more stably stratified water
 376 column. This may have contributed to persistence of the surface water temperature anomalies
 377 and the delayed subduction of the warmer subsurface temperatures (Figure 3a) as speculated by
 378 Scannell et al. (2020). The lower energetic near-inertial currents in 2018/2019 winter could have
 379 also resulted in weaker mixing and less entrainment of colder subsurface water. The resulting

380 strong surface stratification could have contributed to the 2019 MHW.



381
382 **Figure 7. (a)** Total zonal and meridional 35 m currents [cm s^{-1}] and **(b)** near-inertial 35 m
383 current magnitudes [cm s^{-1}] observed from the NOAA surface mooring at OSP. The zonal and
384 meridional current data are shown as a 31-day running average. The red shading represents
385 observed MHW periods.

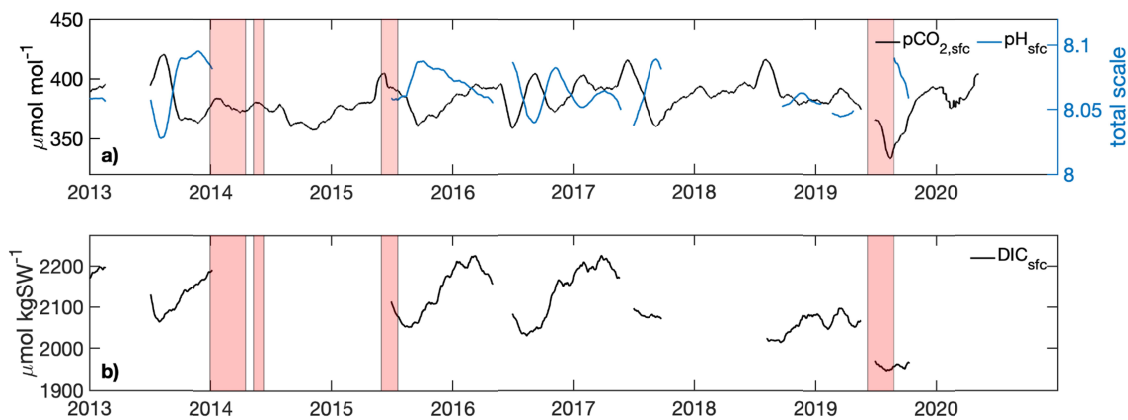
386

387 3.2. Ecosystem Impacts

388

389 Similar to the conditions observed during 2013-2015 MHW (Mogen et al., 2022), we find
390 low surface DIC and $p\text{CO}_2$ along with high surface pH during the 2019 MHW (Figure 8). The
391 strong stratification and circulation changes could have contributed to the decrease in DIC
392 similar to the 2013-2015 MHW (Mogen et al., 2022).

393



394
395 **Figure 8. (a)** Seawater $p\text{CO}_2$ [$\mu\text{mol mol}^{-1}$] and surface seawater pH [total scale] and **(b)** surface
396 dissolved inorganic carbon (DIC) [$\mu\text{mol kgSW}^{-1}$] observed from the NOAA surface mooring at
397 OSP. Data are shown as a 31-day running average. The red shading represents observed MHW
398 periods.

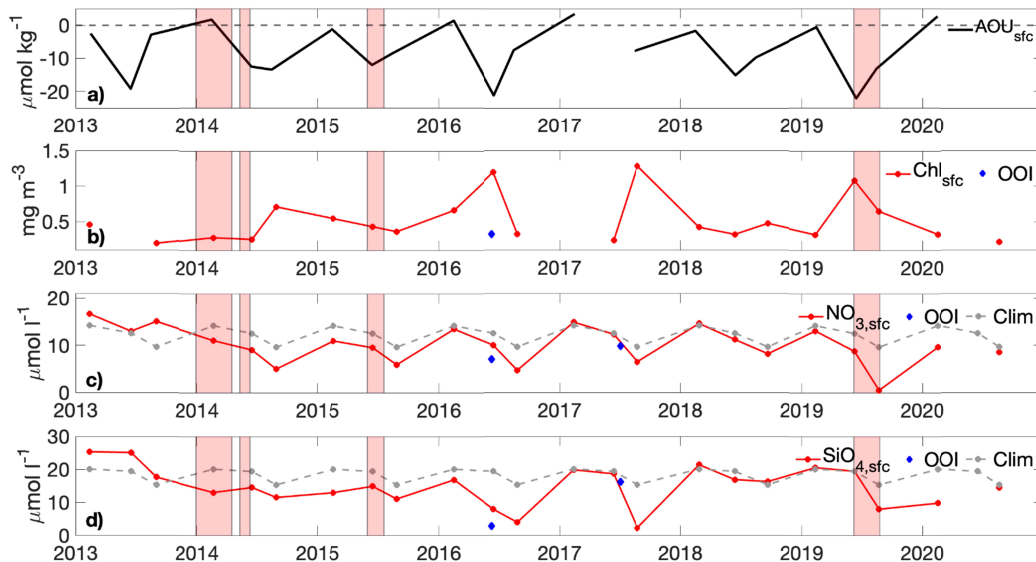
399

400 Relatively large negative Apparent Oxygen Utilization (AOU) (oxygen concentration at
401 saturation equilibrium minus observed oxygen) surface values were observed during the June

402 cruise of 2019 (Figure 9a), suggesting that more oxygen was available in the water than what is
 403 expected based on the water's physical properties, which could be an indication of increased
 404 biological productivity.

405
 406 Surface chlorophyll and macronutrients (nitrate and silicate) from Line P cruises at P26
 407 were used as indicators of productivity occurring at OSP (Figure 9). Notable large amounts of
 408 chlorophyll at OSP were observed in June 2016 (~1.19 mg m⁻³), August 2017 (~1.28 mg m⁻³),
 409 and June 2019 (~1.08 mg m⁻³) as seen in Figure 9b. The large amount of chlorophyll in 2016
 410 coincides with a negative AOU value in Figure 9a and was followed by a decrease in
 411 macronutrients (Figure 9cd). The 2017 chlorophyll bloom occurred directly following the
 412 observed spring barrier layer (Figure 3a), and a decrease in nitrate and a depletion of silicate
 413 were observed directly following as well (Figure 9). The macronutrients again decreased in 2019
 414 (with observed depletion of surface nitrate), coinciding with the observed June 2019 chlorophyll.
 415

416 Typical decreases in surface nitrate (6.9-7 μM) and silicate (11.1-11.5 μM) are indicators
 417 of primary productivity in the Gulf of Alaska (Harrison et al., 1999; Harrison et al., 2004; Wong
 418 et al., 1998). Between the June and August cruises in 2019, there was a 12.6 μM decrease in
 419 nitrate (Figure 9c), almost twice the typical decrease that would follow primary productivity, and
 420 a 12.0 μM decrease in silicate during 2019 (Figure 9d).

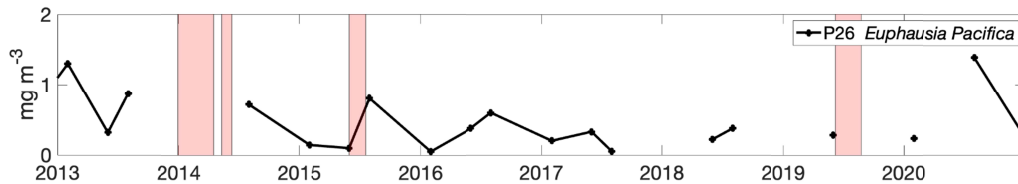


421
 422 **Figure 9.** Surface (a) Apparent Oxygen Utilization (AOU) [$\mu\text{mol mol}^{-1}$] (computed oxygen
 423 concentration at saturation from the NOAA surface mooring at OSP minus observed oxygen
 424 from Line P Station P26 shipboard data), (b) chlorophyll [mg m^{-3}], (c) nitrate [$\mu\text{mol l}^{-1}$], and (d)
 425 silicate [$\mu\text{mol l}^{-1}$]. Line P Station P26 shipboard data are represented in red. OOI shipboard data
 426 are represented as blue diamonds. For nitrate and silicate, the PACIFICA 1985-2008 climatology
 427 is represented as gray dashed lines. The red shading represents observed MHW periods.
 428

429 3.3. Higher Trophic Impacts

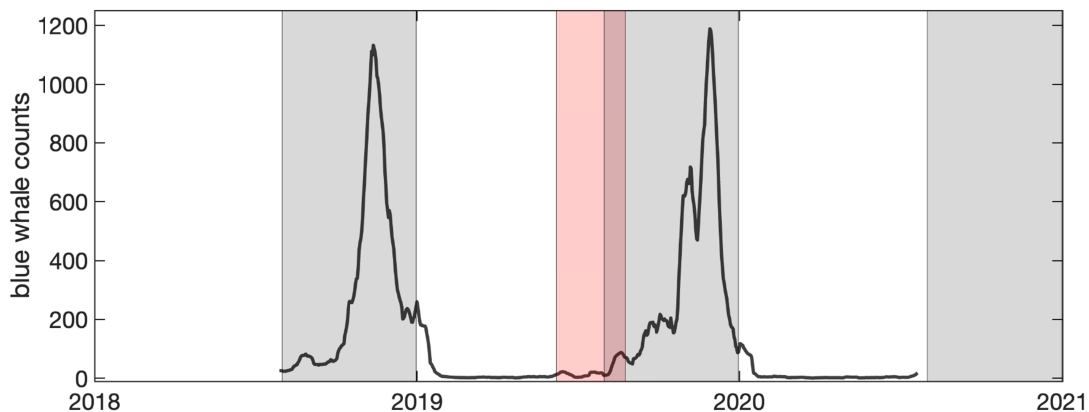
430
 431 We briefly explored other biological data to understand potential relationships with

432 higher trophic levels during the summer of 2019 at OSP. We investigated biomass of *Euphausia*
 433 *pacifica* from Line P's station P26 zooplankton tows (Figure 10). *E. pacifica*, or 'krill', are the
 434 most abundant zooplankton species to the region (Mackas, 1992) and are prey for higher trophic
 435 levels, such as baleen whales. Due to the sparsity of cruise samples taken at P26, there is
 436 insufficient data to understand if the primary productivity and enhanced stratification that
 437 occurred in the summer of 2019 had an impact on *E. pacifica* biomass. However, it is possible
 438 that the data collected by Line P cruises does not fully capture the mobility of *E. pacifica*, as the
 439 anomalous conditions observed in 2019 were likely more widespread rather than localized solely
 440 to OSP. Therefore, we assessed *E. pacifica* biomass on a wider swath (Figure S3) which did
 441 show some similarities to the chlorophyll concentration.
 442



443
 444 **Figure 10.** Shipboard *E. pacifica* biomass [mg m^{-3}] from Line P Station P26 250 m to surface
 445 bongo net. The red shading represents observed MHW periods.
 446

447 OSP's newly added Noise Reference Station's passive acoustic hydrophone allowed us to
 448 capture a glimpse of whale activity surrounding the time of the 2019 MHW (Figure 11). Blue
 449 whales (*Balaenoptera musculus*) have been known to feed as far offshore as OSP (Calambokidis
 450 et al., 2009) and have been observed at OSP most often within Aug-Dec (Stafford et al., 1999).
 451 While the data set is limited in length, in September 2019, there were 38% more blue whale calls
 452 recorded compared to September 2018, suggesting that more blue whales appeared earlier in the
 453 foraging season (Aug to Dec) (Stafford et al., 2007; Stafford et al., 1999). Across the entire
 454 foraging season, more blue whales were present in Aug-Dec 2019 compared to Aug-Dec 2018
 455 (49,879 vs. 45,754 calls) (Figure 11).
 456



457
 458 **Figure 11.** Blue whale B-type calls for July 2018-July 2020 observed from the Noise Reference
 459 Station at OSP. Data are shown as a 15-day running average. The red transparent region
 460 represents the 2019 MHW period. Gray shaded regions represent prospective foraging seasons
 461 (Aug-Dec) of blue whales.

462 **4 Summary**

463 Ocean Station Papa (OSP) provides a unique laboratory for investigating the cascade of
464 offshore impacts of northeast (NE) Pacific MHWs. Although OSP is a point location, many of
465 our observations and conclusions support previous areal-averaged studies of the 2013-2015 and
466 2019 MHWs (Figure 2) (Amaya et al., 2020; Bond et al., 2015; Mogen et al., 2022; Scannell et
467 al., 2020) while providing insight into the widespread impacts of MHWs. OSP provides a unique
468 opportunity to explore the linkages between the physical manifestation of MHWs in the
469 Northeast Pacific and impacts on biogeochemistry and the ecosystem.

470

471 **4.1. Connecting the two most recent MHWs in the northeastern Pacific**

472

473 Subsurface observations (Figure 3 and 4) at OSP provide critical insights into the
474 potential connection between the two recent MHW events along with interactions with the local
475 ecosystems. The water column was stably stratified due to warm and fresh subsurface conditions
476 prior to and during the 2019 MHW. The temperatures at OSP during the peak SST anomalies in
477 summer of 2019 were anomalous throughout the water column, unlike the 2013-2015 MHW
478 where the subsurface temperature anomalies did not reach beyond 150 m (Figure 3a). Subsurface
479 temperature anomalies associated with the 2013-2015 MHW appeared to have been subducted
480 into deeper waters that could have connected the 2013-2015 and 2019 MHWs as previously
481 noted by Scannell et al. (2020). We also found a strong salinity-stratified barrier layer (Figure
482 3a) that persisted between the two MHWs and helped to sustain the deep warm anomalies in-
483 between the events.

484

485 **4.2. Impacts of stratification on biogeochemistry**

486

487 There was a large decrease in surface DIC and $p\text{CO}_2$ along with higher than normal
488 surface pH during the 2019 MHW (Figure 8). The decrease in DIC could have been a result of
489 increased stratification and coincident changes in circulation that were observed in 2019 at OSP,
490 similar to the conditions observed during the 2013-2015 MHW as suggested by Mogen et al.
491 (2022) and Franco et al. (2021); however, the increase in productivity observed in 2019 may
492 have also contributed to this decrease in DIC.

493

494 **4.2. Pre-conditioning of the upper ocean for warm temperatures through a shallow mixed 495 layer and air-sea fluxes**

496

497 The local heat flux anomalies for both the 2013-2015 and 2019 MHWs at OSP were
498 relatively small compared to the area-average values documented by Schmeisser et al. (2019),
499 Amaya et al. (2020), and Bond et al. (2015). OSP is located at the northern edge of the
500 aforementioned studies (as seen in Figure 2ab). However, there were anomalous shortwave
501 radiative fluxes prior to the 2019 MHW and stratification anomalies at OSP. Since the mixed
502 layer is very thin during the summer in the Gulf of Alaska, the perturbations of the mixed layer
503 have a direct influence on the sea surface temperature tendency, and the mixed layer depth
504 perturbation likely dominates the SST variability (Amaya et al., 2020). Thus, the shallow mixed
505 layer and anomalously high shortwave heat flux into the ocean could explain the extreme
506 intensification of the 2019 SST anomalies at OSP.

507

4.3. Impacts of available chemical nutrients and stratification on productivity

Coincident with the increased stratification leading up to the MHW of 2019, there was an increase in primary productivity in June at OSP (relative to prior summer samples taken at Line P Station P26 within 2013- 2020). Line P collected samples at P26 at the beginning (Jun 10) and at the end (Aug 24) of the MHW of 2019 (Jun 8 - Aug 25). In June, there was an increase in chlorophyll and negative AOU, followed by a decrease of silicate and depletion of nitrate in August (Figure 9).

It is likely that there were other processes at play that drove the productivity other than the MHW itself. There was also the possibility of iron enrichment, a limiting factor for larger phytoplankton (Wyatt et al., 2022), which could also have contributed to a large phytoplankton bloom and coincident decreases in nitrate and silicate between the June and August cruises in 2019 (Figure 9). The surface $p\text{CO}_2$ decline and surface pH increase during 2019 at OSP are consistent with $p\text{CO}_2$ and pH observations made during a phytoplankton bloom in the Gulf of Alaska that resulted from volcanic ash iron input in August 2008 (Hamme et al., 2010). Similar to Hamme et al. (2010), there was also evidence of iron deposited from atmospheric dust into surface waters near OSP during the peak of the 2019 MHW (Long et al., 2021; Figure S2). Thus, the MHW's shallow mixed layer might have worked in concert with the iron-enriched dust deposition to support an increase in productivity.

Other recent MHWs have been shown to have negative effects on higher trophic levels closer to shore (Barlow et al., 2023; Cavole et al., 2016). At OSP in 2019, an offshore site, it appears that there might have been a slightly positive effect on higher trophic levels. There was indication that blue whales came earlier in their foraging season and in greater numbers than in the previous year (Figure 11); however, there is not a clear connection between productivity and krill (Figure 10) due to data limitations. The krill data is collected three times a year at Line P's P26 Station, whereas the acoustic data is continuously recorded from all directions surrounding OSP. The different temporal and spatial data collection techniques cause further challenges to connecting blue whale behavior to the krill abundance.

5 Conclusion

The long-term multi-disciplinary time series at OSP allows insight into the evolution and impacts of MHWs. The oceanographic environment at OSP is complex. Interannual and decadal variations in the atmospheric jet stream and Pacific storm track can lead to a wide range of variability in the NE Pacific subarctic gyre and physical environment at OSP. Influences of other processes, such as iron fertilization from wildfires and volcanoes, likely impact the physical, biogeochemical, and ecosystem dynamics at OSP. Due to the relatively short records, gaps, and limited spatial extent in the observational data sets, this analysis should be considered as a case study of the conditions associated with the 2019 NE Pacific MHW at OSP, rather than generalized relationships expected with MHWs at any location. The relationship between the 2019 MHW, increased productivity and the early arrival of blue whales, or increased stratification and de-acidification at OSP should be considered as provocative, rather than definitive. The link to these occurrences may be the enhanced near-surface stratification associated with the MHW, rather than necessarily the extreme temperature itself. The enhanced stratification increased the intensity of the surface forcing on the upper ocean leading to extreme

553 warming. The enhanced stratification also aided in productivity by providing a well-lit and
554 nutrient-available upper ocean to primary producers that led to a bloom in productivity
555 coinciding the extreme temperatures. MHWs can cause a cascade of impacts all over the world,
556 and longer multi-disciplinary time series and time series of MHWs in other regions of the
557 World's oceans are necessary to understand their impacts and interdisciplinary connections.

558 **Acknowledgments**

559 This project would not have been possible without the help and support from the Ocean Climate
560 Stations Group, Acoustics Group, and Carbon Group. Observations were supported by the
561 NOAA NMFS Office of Science and Technology (OST), NOAA Global Ocean Monitoring and
562 Observing (GOMO), DFO Line P Program, NOAA Ocean Acidification Program, and the
563 National Science Foundation. Funding for CK was provided by the NOAA Ernest F. Hollings
564 Undergraduate Scholarship Program, University of Washington, and a fellowship from the
565 American Meteorological Society. This material is also based on the work supported by the
566 National Science Foundation under Grant No. 2022874. This publication is partially funded by
567 the Cooperative Institute for Climate, Ocean, & Ecosystem Studies (CIOCES) under NOAA
568 Cooperative Agreement NA20OAR4320271, Contribution No. 2023-1269. This is PMEL
569 contribution number 5344.

571 **Data Availability**

572 The NOAA surface mooring data, provided by the OCS Group, were obtained from their website
573 at <https://www.pmel.noaa.gov/ocs/>. The PMEL Carbon Group data are available at
574 https://doi.org/10.3334/cdiac/otg.tsm_papa_145w_50n. OOI data are available at the NSF OOI
575 Data Explorer, <https://dataexplorer.oceanobservatories.org/#go-to-data-access>. The wave height
576 data from the APL-UW Waverider Mooring data are available at
577 <https://cdip.ucsd.edu/themes/cdip?pb=1&u2=s:166:st:1&d2=p70>. DFO Line P shipboard data are
578 available at <http://www.pac.dfo-mpo.gc.ca/science/oceans/data-donnees/line-p/index-eng.htm>.
579 OOI cruise data are available at
580 <https://alfresco.oceanobservatories.org/alfresco/faces/jsp/browse/browse.jsp> and
581 <http://ooinet.oceanobservatories.org>. The NOAA OISSTv2.1 High Resolution Dataset data
582 provided by the NOAA PSL, Boulder, Colorado, USA, are available from their website at
583 <https://psl.noaa.gov>. Argo float data were collected and made freely available by the
584 International Argo Program and the national programs that contribute to it and are available at
585 <https://argo.ucsd.edu> and <https://www.ocean-ops.org>. The Argo Program is part of the Global
586 Ocean Observing System.

587 **References**

- 588 Alford, M.H., Cronin, M.F. & Klymak, J.M. (2012). Annual Cycle and Depth Penetration of
589 Wind-Generated Near-Inertial Internal Waves at Ocean Station Papa in the Northeast Pacific.
590 *Journal of Physical Oceanography*, 42(6), 889–909. <https://doi.org/10.1175/jpo-d-11-092.1>
591 Amaya, D.J., Miller, A.J., Xie, S.-P. & Kosaka, Y. (2020). Physical drivers of the summer 2019
592 North Pacific marine heatwave. *Nature Communications*, 11(1).
593 <https://doi.org/10.1038/s41467-020-15820-w>
- 594 Barlow, D.R., Klinck, H., Ponirakis, D., Branch, T.A., & Torres, L.G. (2023). Environmental
595 Conditions and Marine Heatwaves Influence Blue Whale Foraging and Reproductive Effort.
596 *Ecology and Evolution*, 13(2). <https://doi.org/10.1002/ece3.9770>
- 597 Belka, D.J., Schwendeman, M., Thomson, J., & Cronin, M.F. (2014). Historical Wave and Wind
598 Observations at Ocean Station P. *Technical Report no. 1407*. Washington University Seattle
599 Applied Physics Lab, Seattle, WA.
- 600 Benson, B.B. & Krause Jr., D. (1984). The concentration and isotopic fractionation of oxygen
601 dissolved in freshwater and seawater in equilibrium with the atmosphere. *Limnology and*
602 *Oceanography*, 29(3), 620–632. <https://doi.org/10.4319/lo.1984.29.3.0620>
- 603 Bond, N.A., Cronin, M.F., Freeland, H., & Mantua, N. (2015). Causes and impacts of the 2014
604 warm anomaly in the NE Pacific. *Geophysical Research Letters*, 42(9), 3414–3420.
605 <https://doi.org/10.1002/2015gl063306>
- 606 Calambokidis, J., Barlow, J., Ford, J.K.B., Chandler, T.E., & Douglas, A.B. (2009). Insights into
607 the population structure of blue whales in the Eastern North Pacific from recent sightings and
608 photographic identification. *Marine Mammal Science*, 25(4), 816–832.
609 <https://doi.org/10.1111/j.1748-7692.2009.00298.x>
- 610 Capotondi, A., Newman, M., Xu, T., & Di Lorenzo, E. (2022). An Optimal Precursor of
611 Northeast Pacific Marine Heatwaves and Central Pacific El Niño Events. *Geophysical*
612 *Research Letters*, 49(5). <https://doi.org/10.1029/2021gl097350>
- 613 Cavole, L. M., Demko, A. M., Diner, R. E., Giddings, A., Koester, I., Pagniello, C. M. L. S.,
614 Paulsen, M.-L., Ramirez-Valdez, A., Schwenck, S. M., Yen, N. K., Zill, M. E., & Franks, P.
615 J. S. (2016). Biological Impacts of the 2013–2015 Warm-Water Anomaly in the Northeast
616 Pacific: Winners, Losers, and the Future. *Oceanography*, 29(2), 273–285.
617 <https://doi.org/10.5670/oceanog.2016.32>
- 618 Cheung, W.W.L., & Frölicher, T.L. (2020). Marine heatwaves exacerbate climate change
619 impacts for fisheries in the northeast Pacific. *Scientific Reports*, 10(1), 1–10.
620 <https://doi.org/10.1038/s41598-020-63650-z>
- 621 Cronin, M.F., Pelland, N.A., Emerson, S.R., & Crawford, W.R. (2015). Estimating diffusivity
622 from the mixed layer heat and salt balances in the North Pacific. *Journal of Geophysical*
623 *Research: Oceans*, 120(11), 7346–7362. <https://doi.org/10.1002/2015jc011010>
- 624 Cummins, P.F., & Freeland, H.J. (2007). Variability of the North Pacific Current and its
625 bifurcation. *Progress in Oceanography*, 75(2), 253–265.
626 <https://doi.org/10.1016/j.pocean.2007.08.006>
- 627 de Boyer Montégut, C. (2004). Mixed layer depth over the global ocean: An examination of
628 profile data and a profile-based climatology. *Journal of Geophysical Research*, 109(C12).
629 <https://doi.org/10.1029/2004jc002378>
- 630 Di Lorenzo, E., & Mantua, N. (2016). Multi-year persistence of the 2014/15 North Pacific
631 marine heatwave. *Nature Climate Change*, 6(11), 1042–1047.

- 632 <https://doi.org/10.1038/nclimate3082>
- 633 Dickson, A.G. (1990). Standard potential of the reaction: $\text{AgCl(s)} + 12\text{H}_2\text{(g)} = \text{Ag(s)} + \text{HCl(aq)}$,
634 and the standard acidity constant of the ion HSO_4^- in synthetic sea water from 273.15 to
635 318.15 K. *The Journal of Chemical Thermodynamics*, 22(2), 113–127.
636 [https://doi.org/10.1016/0021-9614\(90\)90074-z](https://doi.org/10.1016/0021-9614(90)90074-z)
- 637 Dickson, A.G., & Millero, F.J. (1987). A comparison of the equilibrium constants for the
638 dissociation of carbonic acid in seawater media. *Deep Sea Research Part A. Oceanographic*
639 *Research Papers*, 34(10), 1733–1743. [https://doi.org/10.1016/0198-0149\(87\)90021-5](https://doi.org/10.1016/0198-0149(87)90021-5)
- 640 Dziak, R.P., Lee, W.S., Haxel, J.H., Matsumoto, H., Tepp, G., Lau, T.-K. ., Roche, L., Yun, S.,
641 Lee, C.-K. ., Lee, J., & Yoon, S.-T. (2019). Hydroacoustic, Meteorologic and Seismic
642 Observations of the 2016 Nansen Ice Shelf Calving Event and Iceberg Formation. *Frontiers*
643 *in Earth Science*, 7. <https://doi.org/10.3389/feart.2019.00183>
- 644 Dziak, R.P., Haxel, J.H., Lau, TK. Heimlich, S., Caplan-Auerbach, J., Mellinger, D. K.,
645 Matsumoto, H., & Mate, B. (2017). A pulsed-air model of blue whale B call vocalizations.
646 *Scientific Reports*, 7(9122). <https://doi.org/10.1038/s41598-017-09423-7>
- 647 Fairall, C.W., Bradley, E.F., Hare, J.E., Grachev, A.A., & Edson, J.B. (2003). Bulk
648 Parameterization of Air–Sea Fluxes: Updates and Verification for the COARE Algorithm.
649 *Journal of Climate*, 16(4), 571–591 [https://doi.org/10.1175/1520-0442\(2003\)016<0571:BPOASF>2.0.CO;2](https://doi.org/10.1175/1520-0442(2003)016<0571:BPOASF>2.0.CO;2)
- 650
- 651 Franco, A.C., Ianson, D., Ross, T., Hamme, R.C., Monahan, A.H., Christian, J.R., Davelaar, M.,
652 Johnson, W.K., Miller, L.A., Robert, M., & Tortell, P.D. (2021). Anthropogenic and Climatic
653 Contributions to Observed Carbon System Trends in the Northeast Pacific. *Global*
654 *Biogeochemical Cycles*, 35(7). <https://doi.org/10.1029/2020gb006829>
- 655 Freeland, H. (2007). A short history of Ocean Station Papa and Line P. *Progress in*
656 *Oceanography*, 75(2), 120–125. <https://doi.org/10.1016/j.pocean.2007.08.005>
- 657 Garcia, H.E. & Gordon, L.I. (1992). Oxygen solubility in seawater: Better fitting equations.
658 *Limnology and Oceanography*, 37(6), 1307–1312. <https://doi.org/10.4319/lo.1992.37.6.1307>.
- 659 Garcia, H.E. & Gordon, L.I. (1993). Erratum: Oxygen solubility in seawater: Better fitting
660 equations. *Limnology and Oceanography*, 38(3), 656.
661 <https://doi.org/10.4319/lo.1993.38.3.0643>.
- 662 Hamme, R.C., Webley, P.W., Crawford, W.R., Whitney, F.A., DeGrandpre, M.D., Emerson,
663 S.R., Eriksen, C.C., Giesbrecht, K.E., Gower, J.F.R., Kavanaugh, M.T., Peña, M.A., Sabine,
664 C.L., Batten, S.D., Coogan, L.A., Grundle, D.S., & Lockwood, D. (2010). Volcanic ash fuels
665 anomalous plankton bloom in subarctic northeast Pacific. *Geophysical Research Letters*,
666 37(19). <https://doi.org/10.1029/2010gl044629>
- 667 Harrison, P.J. (2002). Station Papa Time Series: Insights into Ecosystem Dynamics. *Journal of*
668 *Oceanography*, 58(2), 259–264. <https://doi.org/10.1023/a:1015857624562>
- 669 Harrison, P.J., Boyda, P.W., Varela, D.E., Takeda, S., Shiimoto, A., & Odate, T. (1999).
670 Comparison of factors controlling phytoplankton productivity in the NE and NW subarctic
671 Pacific gyres. *Progress in Oceanography*, 43(2-4), 205–234. [https://doi.org/10.1016/s0079-6611\(99\)00015-4](https://doi.org/10.1016/s0079-6611(99)00015-4)
- 672
- 673 Harrison, P.J., Whitney, F.A., Tsuda, A., Saito, H., & Tadokoro, K. (2004). Nutrient and
674 Plankton Dynamics in the NE and NW Gyres of the Subarctic Pacific Ocean. *Journal of*
675 *Oceanography*, 60(1), 93–117. <https://doi.org/10.1023/b:joce.0000038321.57391.2a>
- 676 Hartmann, D.L. (2015). Pacific sea surface temperature and the winter of 2014. *Geophysical*
677 *Research Letters*, 42(6), 1894–1902. <https://doi.org/10.1002/2015gl063083>

- 678 Hayashida, H., Matear, R. J., & Strutton, P. G. (2020). Background Nutrient Concentration
679 Determines Phytoplankton Bloom Response to Marine Heatwaves. *Global Change Biology*,
680 26(9), 4800–4811. <https://doi.org/10.1111/gcb.15255>
- 681 Hobday, A.J., Alexander, L.V., Perkins, S.E., Smale, D.A., Straub, S.C., Oliver, E.C.J.,
682 Benthuyesen, J.A., Burrows, M.T., Donat, M.G., Feng, M., Holbrook, N.J., Moore, P.J.,
683 Scannell, H.A., Sen Gupta, A., & Wernberg, T. (2016). A hierarchical approach to defining
684 marine heatwaves. *Progress in Oceanography*, 141(0079-6611), 227–238.
685 <https://doi.org/10.1016/j.pocean.2015.12.014>
- 686 Holbrook, N.J., Scannell, H.A., Sen Gupta, A., Benthuyesen, J.A., Feng, M., Oliver, E.C.J.,
687 Alexander, L.V., Burrows, M.T., Donat, M.G., Hobday, A.J., Moore, P.J., Perkins-
688 Kirkpatrick, S.E., Smale, D.A., Straub, S.C., & Wernberg, T. (2019). A global assessment of
689 marine heatwaves and their drivers. *Nature Communications*, 10(1).
690 <https://doi.org/10.1038/s41467-019-10206-z>
- 691 Holbrook, N.J., Sen Gupta, A., Oliver, E.C.J., Hobday, A.J., Benthuyesen, J.A., Scannell, H.A.,
692 Smale, D.A., & Wernberg, T. (2020). Keeping pace with marine heatwaves. *Nature Reviews*
693 *Earth & Environment*, 1(9), 482–493. <https://doi.org/10.1038/s43017-020-0068-4>
- 694 Huang, B., Liu, C., Banzon, V., Freeman, E., Graham, G., Hankins, B., Smith, T., & Zhang, H.-
695 M. (2020). Improvements of the Daily Optimum Interpolation Sea Surface Temperature
696 (DOISST) Version 2.1, *Journal of Climate*, 34, 2923-2939. doi: 10.1175/JCLI-D-20-0166.1
697 Accessed Jun 2022.
- 698 Katsura, S., Oka, E., & Sato, K. (2015). Formation Mechanism of Barrier Layer in the
699 Subtropical Pacific. *Journal of Physical Oceanography*, 45(11), 2790–2805.
700 <https://doi.org/10.1175/jpo-d-15-0028.1>
- 701 Lewis, E., & Wallace, D. W. R. (1998). Program Developed for CO2 System Calculations,
702 ORNL/CDIAC-105, *Oak Ridge National Lab*. <https://doi.org/10.15485/1464255>
- 703 Long, J.S., Fassbender, A.J., & Estapa, M.L. (2021). Depth Resolved Net Primary Production in
704 the Northeast Pacific Ocean: A Comparison of Satellite and Profiling Float Estimates in the
705 Context of Two Marine Heatwaves. *Geophysical Research Letters*, 48(19).
706 <https://doi.org/10.1029/2021gl093462>
- 707 Lukas, R., & Lindstrom, E. (1991). The mixed layer of the western equatorial Pacific Ocean.
708 *Journal of Geophysical Research*, 96(S01), 3343. <https://doi.org/10.1029/90jc01951>
- 709 Mackas, D.L. (1992). Seasonal Cycle of Zooplankton off Southwestern British Columbia: 1979–
710 89. *Canadian Journal of Fisheries and Aquatic Sciences*, 49(5), 903–921.
711 <https://doi.org/10.1139/f92-101>
- 712 Mackas, D.L. (1995). Interannual variability of the zooplankton community off southern
713 Vancouver Island. *Climate change and northern fish populations*, 121, 603-615.
- 714 McDougall, T. J. & Barker P.M. (2011). Getting started with TEOS-10 and the Gibbs Seawater
715 (GSW) Oceanographic Toolbox, 28, SCOR/IAPSO WG127, ISBN 978-0-646-55621-5.
- 716 Mehrbach, C., Culbertson, C.H., Hawley, J.E., & Pytkowicz, R.M. (1973). Measurement of The
717 Apparent Dissociation Constants of Carbonic Acid in Seawater at Atmospheric Pressure.
718 *Limnology and Oceanography*, 18(6), 897–907. <https://doi.org/10.4319/lo.1973.18.6.0897>
- 719 Mellinger, D.K. (2001). Ishmael 1.0 User's Guide. NOAA Technical Memorandum OAR
720 PMEL-120. <http://www.pmel.noaa.gov/pubs/PDF/mell2434/mell2434.pdf>. Available from
721 NOAA/PMEL/OERD, 2115 SE OSU Drive, Newport, Oregon.
- 722 Mellinger, D.K. (2004). A comparison of methods for detecting right whale calls. *Canadian*
723 *Acoustics*, 32(55-65).

- 724 Mellinger, D.K., & Clark, C.W. (2000). Recognizing transient low-frequency whale sounds by
725 spectrogram correlation. *The Journal of the Acoustical Society of America*, 107(6), 3518–
726 3529. <https://doi.org/10.1121/1.429434>
- 727 Mogen, S.C., Lovenduski, N.S., Dallmann, A.R., Gregor, L., Sutton, A.J., Bograd, S.J., Quiros,
728 N.C., Di Lorenzo, E., Hazen, E.L., Jacox, M.G., Buil, M.P., & Yeager, S. (2022). Ocean
729 Biogeochemical Signatures of the North Pacific Blob. *Geophysical Research Letters*, 49(9).
730 <https://doi.org/10.1029/2021gl096938>
- 731 Noh, K. M., Lim H.-G., & Kug J.-S. (2022). Global Chlorophyll Responses to Marine
732 Heatwaves in Satellite Ocean Color. *Environmental Research Letters*, 17(6), 064034.
733 <https://doi.org/10.1088/1748-9326/ac70ec>
- 734 Scannell, H.A., Johnson, G.C., Thompson, L., Lyman, J.M., & Riser, S.C. (2020). Subsurface
735 Evolution and Persistence of Marine Heatwaves in the Northeast Pacific. *Geophysical*
736 *Research Letters*, 47(23). <https://doi.org/10.1029/2020gl090548>
- 737 Schmeisser, L., Bond, N.A., Siedlecki, S.A., & Ackerman, T.P. (2019). The Role of Clouds and
738 Surface Heat Fluxes in the Maintenance of the 2013–2016 Northeast Pacific Marine
739 Heatwave. *Journal of Geophysical Research: Atmospheres*, 124(20), 10772–10783.
740 <https://doi.org/10.1029/2019jd030780>
- 741 Smale, D.A., Wernberg, T., Oliver, E.C.J., Thomsen, M., Harvey, B.P., Straub, S.C., Burrows,
742 M.T., Alexander, L.V., Benthuyssen, J.A., Donat, M.G., Feng, M., Hobday, A.J., Holbrook,
743 N.J., Perkins-Kirkpatrick, S.E., Scannell, H.A., Sen Gupta, A., Payne, B.L., & Moore, P.J.
744 (2019). Marine heatwaves threaten global biodiversity and the provision of ecosystem
745 services. *Nature Climate Change*, 9(4), 306–312. <https://doi.org/10.1038/s41558-019-0412-1>
- 746 Stafford, K., Citta, J., Moore, S., Daher, M., & George, J. (2009). Environmental correlates of
747 blue and fin whale call detections in the North Pacific Ocean from 1997 to 2002. *Marine*
748 *Ecology Progress Series*, 395, 37–53. <https://doi.org/10.3354/meps08362>
- 749 Stafford, K.M., Mellinger, D.K., Moore, S.E., & Fox, C.G. (2007). Seasonal variability and
750 detection range modeling of baleen whale calls in the Gulf of Alaska, 1999–2002. *The*
751 *Journal of the Acoustical Society of America*, 122(6), 3378–3390.
752 <https://doi.org/10.1121/1.2799905>
- 753 Stafford, K.M., Nieukirk, S.L., & Fox, C.G. (1999). AN ACOUSTIC LINK BETWEEN BLUE
754 WHALES IN THE EASTERN TROPICAL PACIFIC AND THE NORTHEAST PACIFIC1.
755 *Marine Mammal Science*, 15(4), 1258–1268. [https://doi.org/10.1111/j.1748-
756 7692.1999.tb00889.x](https://doi.org/10.1111/j.1748-7692.1999.tb00889.x)
- 757 Sutton, A.J., Sabine, C.L., Dietrich, C., Maenner-Jones, S., Musielewicz, S., Bott, R., Osborne, J.
758 (2012). High-resolution ocean and atmosphere pCO₂ time-series measurements from
759 mooring Papa_145W_50N in the North Pacific Ocean (NCEI Accession 0100074). [Jan
760 2013- Dec 2020]. NOAA National Centers for Environmental Information. Dataset.
761 https://doi.org/10.3334/cdiac/otg.tsm_papa_145w_50n. Accessed June 2022.
- 762 Sutton, A.J., Sabine, C.L., Feely, R.A., Cai, W.-J., Cronin, M.F., McPhaden, M.J., Morell, J.M.,
763 Newton, J.A., Noh, J.-H., Ólafsdóttir, S.R., Salisbury, J.E., Send, U., Vandemark, D.C., &
764 Weller, R.A. (2016). Using present-day observations to detect when anthropogenic change
765 forces surface ocean carbonate chemistry outside preindustrial bounds. *Biogeosciences*,
766 13(17), 5065–5083. <https://doi.org/10.5194/bg-13-5065-2016>
- 767 Sutton, A.J., Sabine, C.L., Maenner-Jones, S., Lawrence-Slavas, N., Meinig, C., Feely, R.A.,
768 Mathis, J.T., Musielewicz, S., Bott, R., McLain, P.D., Fought, H.J., & Kozyr, A. (2014). A
769 high-frequency atmospheric and seawater pCO₂ data set from 14 open-ocean sites using a

- 770 moored autonomous system. *Earth System Science Data*, 6(2), 353–366.
771 <https://doi.org/10.5194/essd-6-353-2014>
- 772 Suzuki, T., Ishii, M., Aoyama, M., Christian, J., Enyo, K., Kawano, T., Key, R.M., Kosugi, N.,
773 Kozyr, A., Miller, L., Murata, A., Nakano, T., Ono, T., Saino, T., Sasaki, K., Sasano, D.,
774 Takatani, Y., Wakita, M., & Sabine, C.L. (2013). The Pacific Ocean Interior Carbon
775 (PACIFICA) Database (NCEI Accession 0110865). Nitrate, Nitrite, Sulfite, and Oxygen
776 within 49-51°N & 144-146°W. *NOAA National Centers for Environmental Information*.
777 Dataset. <https://doi.org/10.25921/n9nn-8324>. Accessed Jun 2022.
- 778 Thomson, J., D'Asaro, E.A., Cronin, M.F., Rogers, W.E., Harcourt, R.R., & Shcherbina, A.
779 (2013). Waves and the equilibrium range at Ocean Weather Station P. *Journal of*
780 *Geophysical Research: Oceans*, 118(11), 5951–5962. <https://doi.org/10.1002/2013jc008837>
- 781 van Heuven, S., Rae, J.W.B., Wallace, D.W.R., Lewis, E., & Pierrot, D. (2011). MATLAB
782 Program Developed for CO₂ System Calculations. *Carbon Dioxide Information Analysis*
783 *Center*, ORNL/CDIAC-105b. https://doi.org/10.3334/cdiac/otg.co2sys_matlab_v1.1
- 784 Whitney, F., Wong, C., & Boyd, P. (1998). Interannual variability in nitrate supply to surface
785 waters of the Northeast Pacific Ocean. *Marine Ecology Progress Series*, 170, 15–23.
786 <https://doi.org/10.3354/meps170015>
- 787 Whitney, F.A., & Freeland, H.J. (1999). Variability in upper-ocean water properties in the NE
788 Pacific Ocean. *Deep Sea Research Part II: Topical Studies in Oceanography*, 46(11-12),
789 2351–2370. [https://doi.org/10.1016/s0967-0645\(99\)00067-3](https://doi.org/10.1016/s0967-0645(99)00067-3)
- 790 Wong, C.S., Whitney, F.A., Matear, R.J., & Iseki, K. (1998). Enhancement of new production in
791 the northeast subarctic Pacific Ocean during negative North Pacific index events. *Limnology*
792 *and Oceanography*, 43(7), 1418–1426. <https://doi.org/10.4319/lo.1998.43.7.1418>
- 793 Wyatt, A.M., Resplandy, L., & Marchetti, A. (2022). Ecosystem Impacts of Marine Heat Waves
794 in the Northeast Pacific. *Biogeosciences*, 19(24), 5689–5705. [https://doi.org/10.5194/bg-19-](https://doi.org/10.5194/bg-19-5689-2022)
795 [5689-2022](https://doi.org/10.5194/bg-19-5689-2022)